International Journal of Mechanical Engineering and Technology (IJMET)
Volume 10, Issue 02, February 2019, pp. 169-186, Article ID: IJMET_10_02_021
Available online at http://www.iaeme.com/ijmet/issues.asp?JType=IJMET&VType=10&IType=2
ISSN Print: 0976-6340 and ISSN Online: 0976-6359

A COMPARATIVE STUDY OF FLOW AND HEAT TRANSFER CHARACTERISTICS OF STAGGERED AND IN-LINE CROSS-FLOW TUBE-TYPE HEAT EXCHANGERS, PART II: THE FINITE ELEMENT ANALYSIS

***Uguru-Okorie D.C. and Ikpotokin Igbinosa**
Department of Mechanical Engineering
Landmark University, Omu-Aran, Kwara State, Nigeria

David A. Fadare
Department of Mechanical Engineering
University of Ibadan, Oyo State, Nigeria
*corresponding author

ABSTRACT

Numerical analysis of fluid flow and heat transfer were performed for cross-flow tube-type heat exchanger in staggered and in-line arrangement. The purpose of this project was to simulate the process of forced convection heat transfer of air over a heated cylindrical pure copper rod using finite element scheme and compared the results with experimentally obtained data. Also, the work was to compare the performance of both staggered and in-line tube bundle configurations. The cross-flow tube-type heat exchangers consist of 25 mm transverse pitch, 18.75 mm longitudinal pitch, 20 cylindrical rods of Ø12.5 mm in a 125 x 125 mm cross section. Finite element simulation was carried out by modeling the working sections of the cross flow heat exchangers. In this, Model geometry was created, meshed, calculated, and post-processed using FEMLAB 3.0 for ten different air inlet velocities corresponding to experimental data obtained. The simulation results revealed 29.77% and 25.31% deviation in Nusselt number from experimental results for staggered and in-line tube bank respectively

Keywords: forced convective heat transfer, finite element simulation, cross-flow tube-type heat exchanger, staggered tube bank and in-line tube bank.

Cite this Article: Uguru-Okorie D.C, Ikpotokin Igbinosa and David A. Fadare, A Comparative Study of Flow and Heat Transfer Characteristics of Staggered and in-Line Cross-Flow Tube-Type Heat Exchangers, Part II: The Finite Element Analysis, *International Journal of Mechanical Engineering and Technology*, 10(2), 2019, pp. 169-186.
http://www.iaeme.com/IJMET/issues.asp?JType=IJMET&VType=10&IType=2

1. INTRODUCTION

The use of heat exchangers is common in numerous industries where there is a need for heat transfer between different media. Some design parameters are required for optimal design of a heat exchanger, and they include the determination of its operating parameters and performance, the flow and heat transfer characteristics between the fluid flow and the structure of the heat exchanger [1]. The performance of a heat exchanger can be determined directly by experimental measurements [2, 3] or by numerical simulations using different mathematical models [4].

The experimental studies are less appealing because of the high time and cost involved and, this makes this method less appealing and suited for the comprehensive parametrical analysis of diverse heat exchanger prototypes. However, for the development of heat exchangers, to meet the required industrial needs, comprehensive parametrical analyses are needed. As a result, experimental works are being increasingly complemented by different numerical methods and approaches, for the determination of the performance of developed heat exchangers [1].

Despite the fast emerging high speed of the modern day digital computers, Numerical simulations of fluid flow and heat transfer behaviour are still computationally too demanding. Horvat and Mavko [5] have made significant contributions in simplifying the modeling process. The purpose of this work is to investigate the possibilities for determining the heat transfer coefficient and flow characteristics between cylindrical copper element and the air flowing past it in different tube banks. Two different tubes arrangement; staggered and in-line tubes arrangement. A commercial finite element code FEMLAB 3.0 was used for this analysis and the results were compared with experimentally obtained data. In the analysis ten different inlet velocities were considered.

2. LITERATURE REVIEW

Fluid flows in cross-flow tube-type heat exchangers are either laminar or turbulent. Laminar flows are well-ordered and are characterized by the sliding of one fluid layer over another. On the other hand, turbulent flows are rather eddying and chaotic even at the macroscopic level [6]. Computational fluid dynamics (CFD) facilitates the numerical simulation of fluid flow features by solving appropriate partial differential equations. Contrary to the revolutionary pace of CFD, developments in flow modeling (e.g turbulence) have been only evolutionary and the resulting pace of improvement has frustrated the CFD community [7]. This frustration results from the lack of clear choice for a general turbulence model. With the advances in modern days digital computers, so has the range and size of tasks demanded of them. As larger and much faster machines are invented, more complex flow models will be applied. Hence, bigger, faster and less expensive computers will always be sought after. However, if maximum benefit is to be obtained, three major areas need attention. They include computational algorithms, methods of dealing with complex geometries and turbulence models [8].

Numerical simulations are not theoretical solutions but are experimental ones, parallel to those realized in the laboratory [9]. Kelkar & Patankar [10] performed a linear stability analysis and predicted the onset of unsteadiness arising out of vortex shedding. An understanding of the laminar flow past a circular cylinder forms the first step towards understanding the vastly more complicated phenomenon of turbulence [11]. Thus, the simulation of flow past a circular cylinder in a channel becomes a mandatory first step to the more complex tube bundle problem. An extensive experimental review on flow past tube banks was given by Zukauskas [2]. Though the advances in computation are on the increase, the real life practical range of parameters and operating conditions are much more complex than can be numerically simulated. However, these difficulties and complexities have not dampened the spirit of the CFD community. They have made some reasonable assumptions and obtained some useful solutions valid for practical designs. Launder & Massey [4] and Fuji et. al. [12] have employed a finite difference technique, while Dhaubhadel et. al.[13] have used penalty function finite element methods for the simulation of tube bank flows. Gowda et. al. [14] carried out finite element simulations of transient laminar flow past an in-line tube bank for a Reynolds number of 100. They solved two-dimensional unsteady Navier-Stokes and energy equations using an explicit and a semi-implicit algorithm for selected Reynolds and Prandtl numbers.

3. MATERIALS AND METHODS

3.1. Models description

The physical models for flow past five rows of four column staggered and in-line tube banks are shown in figure 3.1 and 3.2 respectively. These models provide thermal analysis of a heated rod of cylindrical shape subject to cross flow of air. Each model consists of a forced-cooled heated element and 20 circular tubes positioned in an enclosure of 125 X 125mm. The square domain represents the air flow field. The cross section of the heated rod is a disk and it is inserted into the domain to model cross flow.

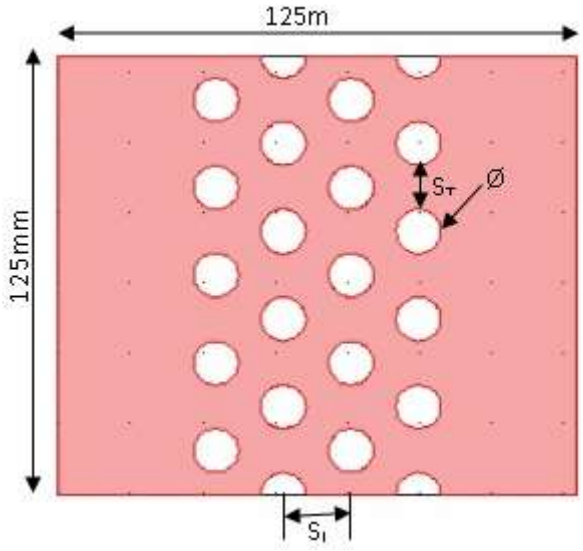

Figure 3.1 Illustration of main computational domain and geometric parameters of the staggered tube bank heat exchanger numerical model.

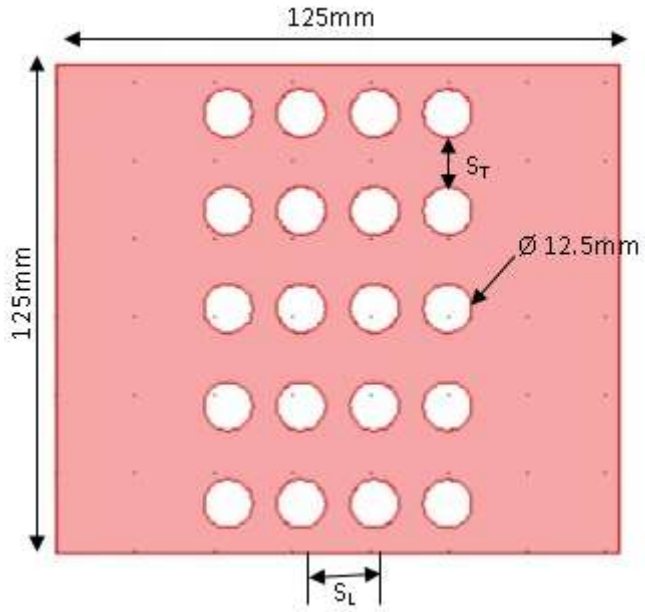

Figure 3.2 Illustration of main computational domain and geometric parameters of the in-line tube bank heat exchanger numerical model.

The diameter of each tube is 12.5mm and the height is 95mm. The longitudinal and transverse pitches are 18.75mm and 25mm respectively. To simulate a typical cross flow over tube banks, the governing equations were deactivated in the circular domain representing the cylindrical rods and the heated element. The average heat transfer coefficient is to be determined and compared with the experimental results.

3.2. Mathematical model

The governing equations for this project are the continuity, Navier-Stokes for momentum and energy equations for steady-state flow, and can be written (generally) as follows:

Continuity equation:

$$\frac{\partial U_i}{\partial X_i} = 0 \tag{3.1}$$

Momentum equations (in *Xi* direction):

$$\ell\left[\frac{\partial U_i}{\partial \tau} + U_j \frac{\partial U_i}{\partial X_j}\right] = -\frac{\partial P}{\partial X_i} + F_i + \frac{\partial}{\partial X_j}\left[\mu\left(\frac{\partial U_i}{\partial X_j} + \frac{\partial U_j}{\partial X_i}\right)\right] \tag{3.2}$$

Energy equation:

$$\ell C_p\left[\frac{\partial T_i}{\partial \tau} + U_j \frac{\partial T_i}{\partial X_j}\right] = \frac{\partial}{\partial X_j}\left(K \frac{\partial T}{\partial X_j}\right) \tag{3.3}$$

where j = 1, 2 for plane and axi-symmetric flows. In the above equations, P is the static pressure, density (ℓ) and time (τ).

For this project the two-dimensional forced flow of Newtonian, constant properties and incompressible fluid are assumed, therefore, equation (3.1) can be written in form:

$$\frac{\partial U}{\partial x}+\frac{\partial V}{\partial y}=0 \tag{3.4}$$

equation (3.2) can be written in form:

$$\ell\left[\frac{\partial U}{\partial \tau}+U\frac{\partial U}{\partial x}+V\frac{\partial U}{\partial y}\right]=-\frac{\partial P}{\partial x}+\mu\left(\frac{\partial^2 U}{\partial x^2}+\frac{\partial^2 U}{\partial y^2}\right)+F_x \tag{3.5a}$$

$$\ell\left[\frac{\partial V}{\partial \tau}+U\frac{\partial V}{\partial x}+V\frac{\partial V}{\partial y}\right]=-\frac{\partial P}{\partial y}+\mu\left(\frac{\partial^2 V}{\partial x^2}+\frac{\partial^2 V}{\partial y^2}\right)+F_y \tag{3.5b}$$

and equation (3.3) can be written in form:

$$\ell C_p\left[\frac{\partial T}{\partial \tau}+u\frac{\partial T}{\partial x}\right]=K\left(\frac{\partial^2 T}{\partial x^2}+\frac{\partial^2 T}{\partial y^2}\right) \tag{3.6}$$

The Galerkin formulation uses the shape functions as the weight functions. The finite element shape functions are discussed by Fletcher [15] and Segarlind [16]. Linear triangular elements (with *i*, *j*, *k* as subscripts) are used to represent *U*, *V*, *P* and *T*, which are approximated as:

$$\begin{aligned} U &= N_i U_i + N_j U_j + N_k U_k; \\ V &= N_i V_i + N_j V_j + N_k V_k; \\ P &= N_i P_i + N_j P_j + N_k P_k; \\ T &= N_i T_i + N_j T_j + N_k T_k. \end{aligned} \tag{3.7}$$

If the Galerkin method is applied to equation (3.4) on elemental basis, we obtain integral form

$$\int_{A^e} N^T\left(\frac{\partial U}{\partial x}+\frac{\partial V}{\partial y}\right)t\,dx\,dy=0 \tag{3.8}$$

where the thickness is introduced so that each term in equation (3.8) has dimensions of volume per unit time. Let t be unity and

$$U = Na_u^e \tag{3.9a}$$

$$V = Na_v^e \tag{3.9b}$$

where a_u^e and a_v^e are given by

$$a_u^e = \left[U_i, U_j, U_k\right]^T \tag{3.10a}$$

and

$$a_v^e = \left[V_i, V_j, V_k\right]^T \tag{3.11b}$$

for the triangular element.

In equation (3.10a) U_i, U_j, U_k are the *X and Y* component of velocity at nodes *i, j and k*. Since a_u^e and a_v^e are independent of *X and Y*, equation (3.8) can be written in matrix form as:

$$K_u^e a_u^e + K_v^e a_v^e = 0 \tag{3.12}$$

where

$$K_u^e = \int_{A^e} N^T \frac{\partial N}{\partial x} t dx dy \tag{3.13}$$

$$K_v^e = \int_{A^e} N^T \frac{\partial N}{\partial y} t dx dy \tag{3.14}$$

Using the Galerkin method, equation (3.5a) can be written in integral form

$$\int_{A^e} N^T \left[\ell \left(\frac{\partial U}{\partial \tau} + U \frac{\partial U}{\partial x} + V \frac{\partial U}{\partial y} \right) + \frac{\partial P}{\partial x} - \mu \left(\frac{\partial^2 U}{\partial x^2} + \frac{\partial^2 U}{\partial y^2} \right) - F_x \right] t dx dy = 0 \tag{3.15}$$

If we represent the pressure *p* over element by

$$P = N a_p^e \tag{3.16}$$

$$U = N a_u^e(\tau) \tag{3.17a}$$

$$V = N a_v^e(\tau) \tag{3.17b}$$

Then equation (3.15) can be written in matrix form

$$C_u^e a_u^e + K_{uu}^e a_u^e + K_{vu}^e a_u^e + K_{ux}^e a_u^e + K_{uy}^e a_u^e + K_{px}^e a_p^e = f_x^e \tag{3.18}$$

Where

$$C_u^e = \int_{A^e} N^T N \ell dx dy \tag{3.19a}$$

$$K_{uu}^e = \int_{A^e} N^T \ell N a_u^e \frac{\partial N}{\partial x} t dx dy \tag{3.19b}$$

$$K_{vu}^e = \int_{A^e} N^T \ell N a_v^e \frac{\partial N}{\partial y} t dx dy \tag{3.19c}$$

$$K_{ux}^e = \int_{A^e} \frac{\partial N^T}{\partial x} \mu \frac{\partial N}{\partial x} t dx dy \tag{3.19d}$$

$$K_{uy}^e = \int_{A^e} \frac{\partial N^T}{\partial y} \mu \frac{\partial N}{\partial y} t dx dy \tag{3.19e}$$

$$K_{px}^e = \int_{A^e} N^T \frac{\partial N}{\partial x} t dx dy \tag{3.19f}$$

And

$$f_x^e = \int_{A^e} N^T F_x t dx dy \tag{3.19g}$$

Similarly, applying the Galerkin method to equation (3.5b) gives

$$C_v^e a_v^e + K_{uv}^e a_v^e + K_{vv}^e a_v^e + K_{vx}^e a_v^e + K_{vy}^e a_v^e + Kya_p^e = f_y^e \tag{3.20}$$

Where

$$C_v^e = \int_{A^e} N^T N \ell dxdy \tag{3.21a}$$

$$K_{uv}^e = K_{uu}^e = \int_{A^e} N^T \ell N a_u^e \frac{\partial N}{\partial x} t dxdy \tag{3.21b}$$

$$K_{vv}^e = K_{vu}^e = \int_{A^e} N^T \ell N a_v^e \frac{\partial N}{\partial y} t dxdy \tag{3.21c}$$

$$K_{vx}^e = K_{ux}^e = \int_{A^e} \frac{\partial N^T}{\partial x} \mu \frac{\partial N}{\partial x} t dxdy \tag{3.21d}$$

$$K_{vy}^e = K_{uy}^e = \int_{A^e} \frac{\partial N^T}{\partial y} \mu \frac{\partial N}{\partial y} t dxdy \tag{3.21e}$$

$$K_{py}^e = \int_{A^e} N^T \frac{\partial N}{\partial y} t dxdy \tag{3.21f}$$

And

$$f_y^e = \int_{A^e} N^T F_y t dxdy \tag{3.21g}$$

On an elemental basis also, the Galerkin method applied to equation (3.6) gives

$$\int_{A^e} N^T \left[\ell C_p \left(\frac{\partial T}{\partial \tau} + U \frac{\partial T}{\partial x} \right) - K \left(\frac{\partial^2 T}{\partial x^2} + \frac{\partial^2 T}{\partial y^2} \right) \right] t dxdy = 0 \tag{3.22}$$

Taking t to be unity and combining the boundary integrals gives

$$\int_{A^e} N^T \ell C_p \frac{\partial T}{\partial \tau} t dxdy + \int_{A^e} N^T \ell C_p U \frac{\partial T}{\partial x} t dxdy + \int_{A^e} N^T q_n t dC + \int_{A^e} N^T \frac{\partial T}{\partial x} Kt \frac{\partial T}{\partial x} dxdy + \int_{A^e} N^T \frac{\partial T}{\partial y} Kt \frac{\partial T}{\partial y} dxdy = 0 \tag{3.23}$$

If we imposed the heat fluxes q_{sB} on the global boundary in the direction towards the fluid, then we obtain

$$q_n = -q_{sB} \tag{3.24}$$

Writing T on elemental basis we have

$$T = N a^e(\tau) \tag{3.25}$$

So that equation (3.22) can be written in matrix form

$$C^e a^e + K_{xx}^e a^e + K_{yy}^e a^e + K_u^e a^e = f^e \tag{3.26}$$

where

$$C^e = \int_{A^e} N^T \ell C_p U N dxdy \tag{3.27a}$$

$$K_u^e = \int_{A^e} N^T \ell C_p U t \frac{\partial N}{\partial x} dxdy \tag{3.27b}$$

$$K_{xx}^{e} = \int_{A^e} \frac{\partial N^T}{\partial x} Kt \frac{\partial N}{\partial x} dxdy \tag{3.27c}$$

$$K_{yy}^{e} = \int_{A^e} \frac{\partial N^T}{\partial y} Kt \frac{\partial N}{\partial y} dxdy \tag{3.27d}$$

and

$$f^{e} = \int_{A^e} N^T q_{sB} t dC \tag{3.27e}$$

Where $[N^T] = (N_i, N_j, N_k)$ is the vector of basis or shape functions for the element, C^e is element capacitance matrix, K^e is element stiffness matrix and f^e is the element nodal force vector. The algebraic system of (3.19)–(3.27) together with appropriate boundary conditions can then be solved. The shape functions (N_i, N_j, N_k) for a linear triangular element are defined by the following equation.

$$N_i = a_i + b_i X + c_i Y,\ I = 1, 2, 3 \tag{3.28}$$

$$a_i = X_j Y_k - X_k Y_j;\ b_i = Y_j - Y_k;\ c_i = X_k - X_j,\ i, j, k = 1, 2, 3.$$

In the above equations, X and Y refer to the global coordinates of the fluid flow domain. After obtaining velocities, pressures and temperatures over the computational domain, the locally available information on primitive variables is used to obtain the required design parameters of interest, such as skin friction coefficient, pressure drop, Nusselt number etc.

3.3. Modeling Considerations

1. The geometry for of the heat exchangers arrangement consists of 5 rows and 4 columns was considered for analysis.
2. The tube is modeled as solid blockage, whereas, the square domain in which the tubes have been embedded was modeled as the flow field with gaseous properties to allow the ambient air to pass through it.
3. Conduction takes place from the tube wall and convection takes from the surface of tube. Temperature and flow distributions have been considered to be two dimensional.
4. Ten numerical simulations were performed for Reynolds numbers of 3543, 8680, 11753, 14175, 16367, 18184, 19836, 21418, 22856 and 24380 correspond to 10, 20, 30, 40, 50, 60, 70, 80, 90 and 100% throttle opening respectively. Air inlet velocity U_o is calculated for each simulation.

3.4. Assumptions in modeling

1. Heat is lost from the top surface of heat exchanger by forced convection.
2. Heat loss by radiation from heat exchanger surface is neglected.

3.5. Boundary Conditions

The following boundary conditions were employed during the simulation.

a) Inlet – uniform flow
   i. Velocity of air $U.n = U_0$
   ii. Tangential velocity $V.n = V_0 = 0$
   iii. Temperature of air, $T_A = T_o$

b) Exit or oulet
   i. Pressure, P = 0
   ii. Convective heat flux q.n = 0

c) Cylinder surface
   i. No – slip conditions for Navier – stokes u = 0
   ii. Constant Temperature $T = T_w = 90^oC$ for the heated rod.
   iii. Thermal insulation for boundaries other than the preceding conditions.

Table 3.1 Properties of air at *27^oC (300^ok).*

Name	Expression	Explanation
Eta	$1.846x10^{-5}$	Dynamic viscosity
Rho	1.1614	Density
T_A	27	Air inlet temperature
C_p	1007	Heat capacity
K	0.0263	Thermal conductivity
Q	0	Heat source

where T_w is the heated rod surface temperature.

3.6. Mesh generation

In FEMLAB 3.0, the mesh generator is completely automatic, and generates three nodes triangular element when the mesh button is selected. Figures 3.3 and 3.4 shown the finer mesh generated for the staggered and in-line tube banks models respectively. However, when control over the mesh is desired, it can be obtained in a number of ways. The maximum size of elements in each direction can be specified, along with the maximum height of an element away from an object. If further control is desired, a number of parameters can be given for each object that controls the nature of the mesh around it.

The following steps were used to generate fine mesh:

1. specify the grid type and generate a coarse mesh
2. examine the coarse mesh on a cross-section of the model
3. generate a finer mesh and check the quality with respect to aspect ratio, face alignment, and element volume
4. change mesh parameters if the element aspect ratio or the face alignment is less than 0.15 or if the element volume is on the order of 10−12 or lower and check the quality of the mesh again.

The domain for staggered arrangement model was discritised into 11,347 triangular elements of 55,010 number of degree of freedom by choosing “finer” from the mesh menu. For the in-line configuration model, 11,082 triangular elements with 53,215 number of degree of freedom were produced using the same mesh parameters.

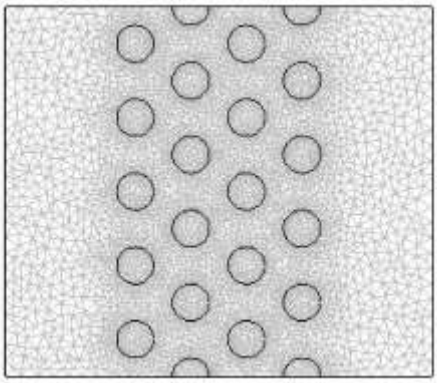

Figure 3.3 Staggered tube model mesh made up of 11,347 triangular elements and 55,010 number of degree of freedom.

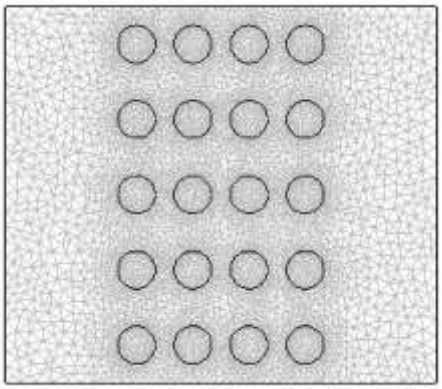

Figure 3.4 In-line tube model mesh made up of 11,082 triangular elements with 53,215 number of degree of freedom.

3.7. Computing the solution

Setting up and running the flow solver, in FEMLAB, is also quite simple. In general, the default parameters which are computed by FEMLAB for the solution are adequate, and, just like for mesh generation, a single button click is enough to perform the simulation. There is no convergence graph to show how the solution is progressing as a function of time. The continuity *residual* is not quite converged, but since it has leveled off very close to the $1e{-}3$ tolerance and the others are well below the convergence tolerance, it can be considered that the solution is effectively converged.

The solver type parametric nonlinear in the solver parameters dialog box was selected. The values of inlet velocity U_0*=4.524, 11.082, 15.005, 18.097, 20.896, 23.216, 25.325, 27.345, 29.180 and 31.126m/s* corresponding to 10, 20 30, 40, 50, 60, 70, 80, 90 and 100% throttle opening were entered into the "Name of parameter" edit field in the list of "parameter values" edit field. The solve toolbar button was clicked. The default plot of velocity distributions for each velocity was produced.

4. RESULTS AND DISCUSSION

In this section, fluid flow and heat transfer characteristics associated with flow normal to staggered and in-line to tubes banks configurations of direct relevance and application in heat exchangers are presented. A complete set of tests were taken with the heated element at the

centre in each of the four ranks of tubes and with ten different inlet velocities. At the heat exchangers' working sections, air is heated by absorbing heat from the heated element.

4.1. Velocity distribution

Streamline patterns after reaching steady state are depicted in figures 4.1 and 4.2 for staggered and in-line tube bank respectively for 50% opening corresponding to 16367 Reynolds numbers. The air enters at the inlet on the left and flows in the direction of the arrows; flows separate from the upstream cylinder downstream body and exits at the outlet on the right-hand side.

In all the ten cases, as the air flows around the first tube bank, it begins to speed up and then the air velocity increases again as it goes around the tube bank downstream of the first. This is verified by the samples taken in the case files for average velocities at the minimum free-flow areas, which showed that the velocity going around the tube downstream is faster than that going around the first tube. The minimum free-flow area is the area of the heat exchanger between two transverse tubes. The flow is forced to speed up, as the tubes act as a type of pipe contraction in the air flow channel.

With inlet velocity of 4.524 m/s, the top velocity at the other subsequent bank is 6.294 m/s, nearly 1.5 times the inlet velocity. For the 20.896 m/s inlet flow case, the top velocity reaches 31.888 m/s, more than 1.5 the inlet velocity. And for the 31.126 m/s inlet case, the top velocity reaches 45.533 m/s, nearly 1.5 times the inlet velocity.

The streamline plots also revealed that vortex formation occurs in the zones of recirculation which is the gap region between cylinders. However, the region is much larger behind the last row of cylinders for low Reynolds number. At high Reynolds number, the vortex is completely washed away after the last row and reappears as the Reynolds number increases further.

4.2. Temperature distribution

Figures 4.3 and 4.4 show the temperature distribution for Reynolds numbers 16367 corresponding to 50% throttle openings for staggered and in-line tube banks respectively after reaching steady state when the heated element was in row one. It is observed that isotherms crowded over the front half of the first row of cylinders. This is because boundary layer growth begins only from the first cylinder.

The largest temperature changes for this case occur in the recirculation and slow velocity just after each of the tubes. The slow-moving areas of the heat exchanger are also better able to absorb heat.

The heat transfer characteristic parameter Nusselt number was calculated from the simulation results for the geometrical flow model from equations (4.1) and (4.2).

$$h = \frac{K_f}{D}\frac{T_w - T_{in}}{T_w - T_b}\left.\frac{\partial T}{\partial Y}\right|_{Y=R} \tag{4.1}$$

$$Nu = \frac{T_w - T_{in}}{T_w - T_b}\left.\frac{\partial T}{\partial Y}\right|_{Y=R} \tag{4.2}$$

Where K_f is the fluid thermal conductivity, T_{in} is the fluid inlet temperature, T_b is the bulk temperature at the minimum cross section and $\frac{\partial T}{\partial Y}$ is the temperature gradient.

The results of local Nusselt number is shown in table 4.1 and 4.2 for staggered and in-line tube banks respectively. The results are also shown graphically in figure 4.5 and 4.6

respectively. It is observed that the local Nuselt number distribution for the first row differs from those of the second and subsequent rows. This is due to the absence of wake shading influence on the first row of cylinder, unlike the rest. The thinner thermal boundary layer over the first row of cylinders leads to a higher temperature gradient and thus, higher heat transfer. Over the first cylinder, the minimum Nu in the plot corresponds to the point of separation. The zones of recirculation come into contact on one side, thus, increased resistance to heat flow and, hence, the smaller values of local Nu.

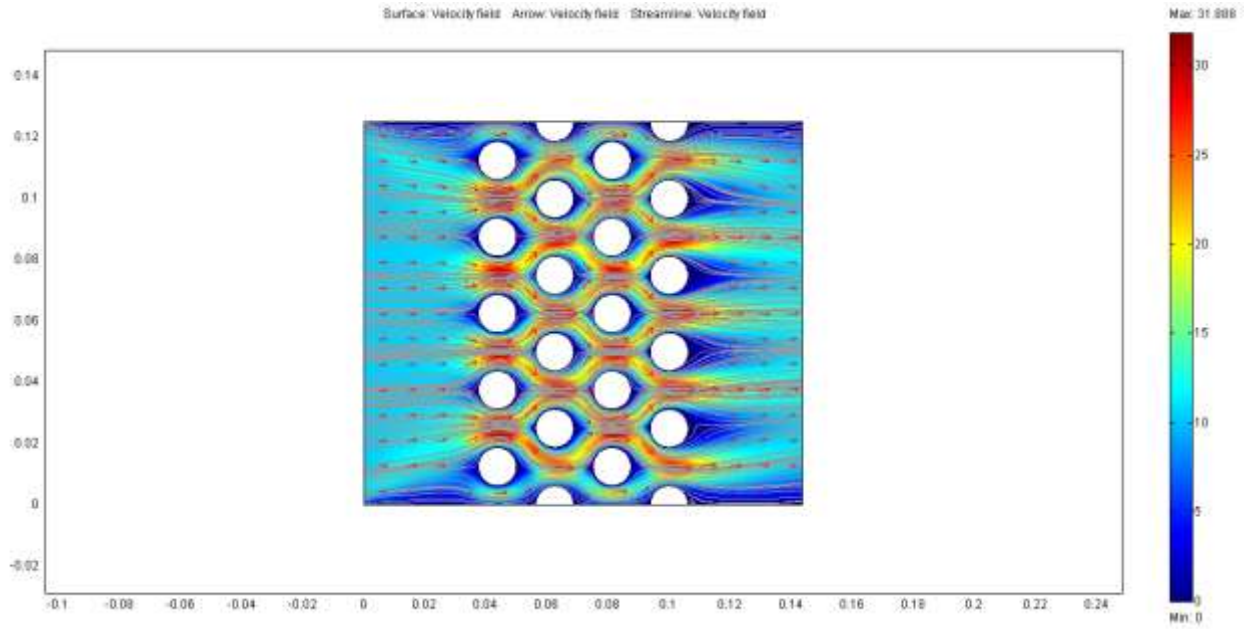

Figure 4.1 50% throttle opening velocity distribution for staggered tube bank

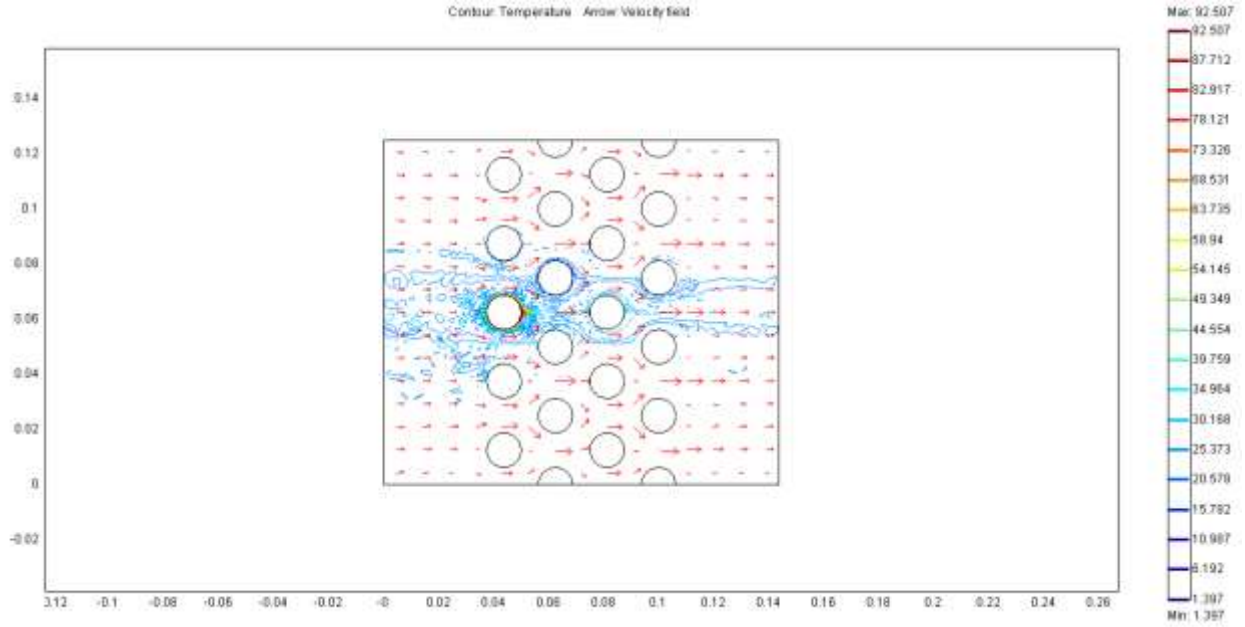

Figure 4.3 50% throttle opening temperature distribution for staggered tube bank

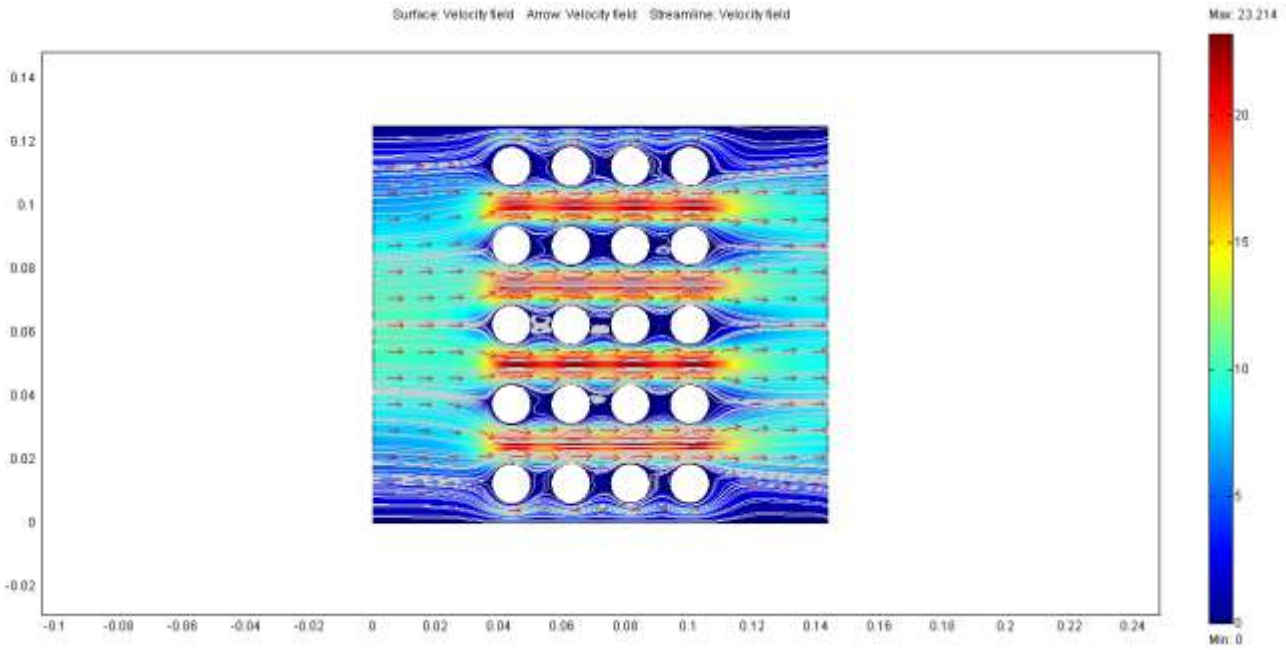

Figure 4.2 50% throttle opening velocity distribution for in-line tube bank

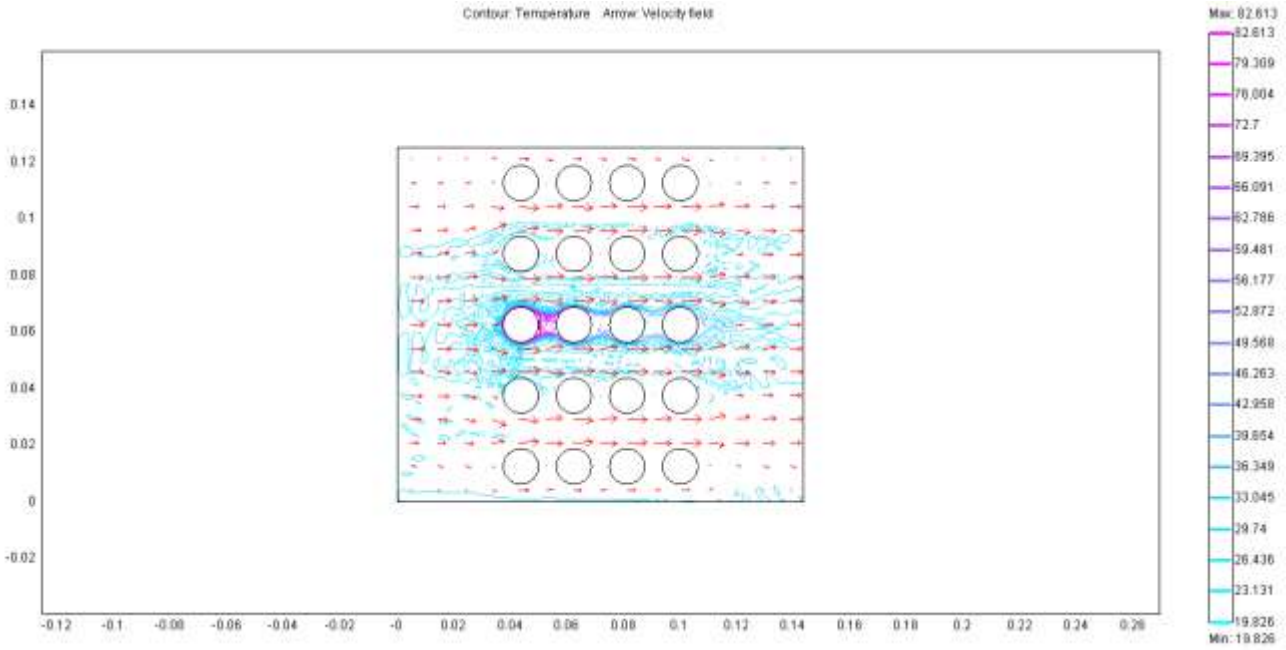

Figure 4.4 50% throttle opening temperature distribution for in-line tube bank

Table 4.1 Numerical results of heat transfer characteristics for the staggered tube bank.

		Row one		**Row two**		**Row three**		**Row four**	
Throttle opening (%)	Re	h	Nu	h	Nu	h	Nu	h	Nu
10	3543	43.97972	20.8193	44.02645	20.84142	44.13293	20.89182	44.32787	20.98411
20	8680	69.64093	32.96691	63.45124	30.0368	61.91511	29.30963	61.90589	29.30526
30	11753	115.318	54.58971	108.7805	51.49494	106.3166	50.32856	107.3521	50.81879
40	14175	138.1975	65.42051	128.6192	60.88628	124.888	59.12001	126.3739	59.82337
50	16367	157.9882	74.78908	145.8784	69.0565	140.3607	66.44454	142.8891	67.64144
60	18184	174.9329	82.81046	159.6808	75.59033	153.4244	72.62864	156.3643	74.02037
70	19836	189.7018	89.80179	171.5756	81.22114	164.4935	77.86858	168.3616	79.69969
80	21418	203.6968	96.42682	183.1596	86.70481	174.7734	82.73494	179.2628	84.86014
90	22856	216.2879	102.3872	193.2212	91.46783	183.865	87.03873	188.8826	89.41399
100	24380	229.5597	108.6699	203.5786	96.37087	193.3465	91.52716	199.3379	94.36339

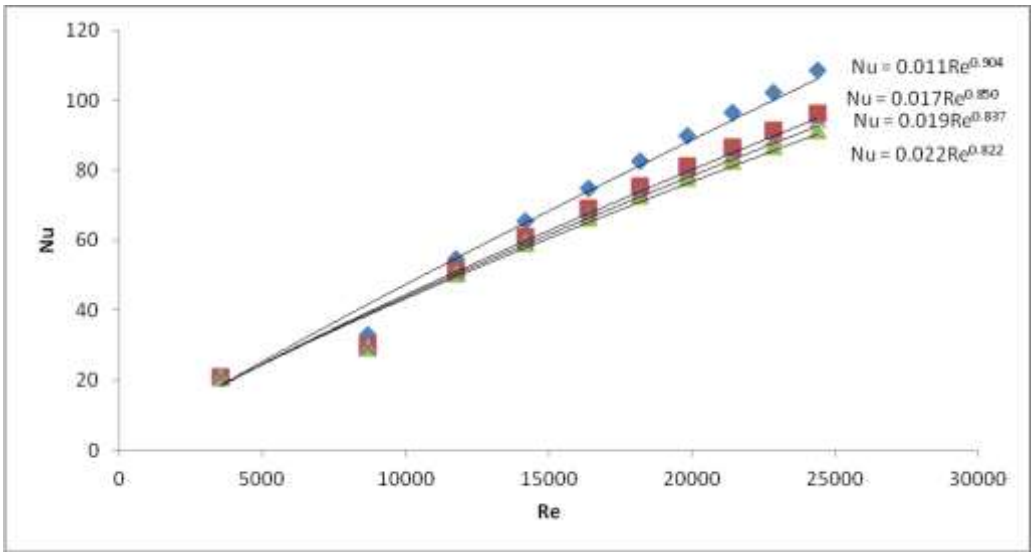

Figure 4.5 Numerical results showing the relationship between (Nu) and (Re) for flow past tube banks of staggered configuration.

Table 4.2 Numerical results of heat transfer characteristics for the in-line tube bank arrangement.

		Row one		**Row two**		**Row three**		**Row four**	
Throttle opening (%)	Re	h	Nu	h	Nu	h	Nu	h	Nu
10	3543	39.9306	18.90251	39.91163	18.89353	39.364	18.63429	40.9586	19.38915
20	8680	59.39635	28.11729	61.11259	28.92973	59.54769	28.18892	63.77579	30.19044
30	11753	78.57573	37.1965	78.57573	37.1965	78.87899	37.34006	85.92344	40.67479
40	14175	92.83956	43.94876	98.79843	46.7696	87.55884	41.44896	103.9929	49.22858
50	16367	105.2277	49.81313	113.1633	53.56972	106.3398	50.33956	120.626	57.10243
60	18184	115.0933	54.48334	124.7181	59.03958	116.7859	55.28459	136.3088	64.52643
70	19836	123.7858	58.59822	134.9381	63.87755	126.1681	59.72595	147.9093	70.0179
80	21418	131.8981	62.43847	144.4891	68.39885	135.1103	63.95904	162.9943	77.15889
90	22856	139.0812	65.83884	152.9278	72.3936	143.2131	67.79479	173.027	81.9082
100	24380	146.5516	69.37518	161.661	76.52775	151.8358	71.87665	188.6722	89.31439

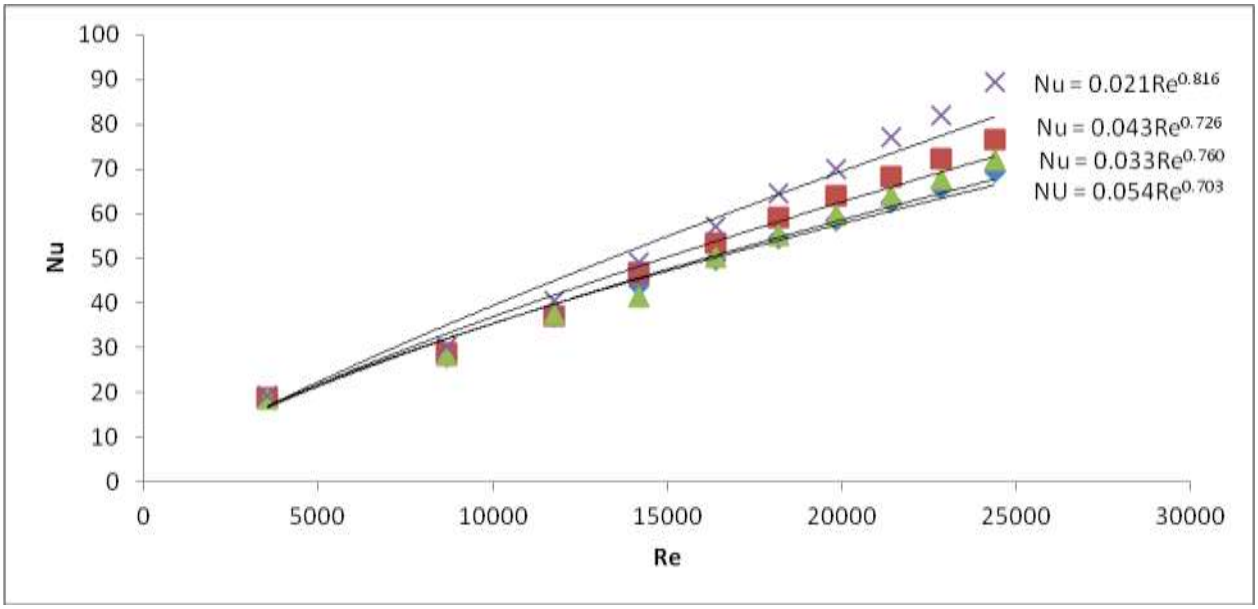

Figure 4.6 Numerical results showing the relationship between (Nu) and (Re) for flow past tube banks of in-line configuration.

4.3. COMPARATIVE ANALYSIS OF THE HEAT EXCHANGERS PERFORMANCE

The numerical results were compared to experimental data as shown in table 4.3 and 4.4 for staggered and in-line tube arrangements respectively. The local Nusselt number of numerical simulation compared satisfactorily to the experimentally obtained values for the whole range of Reynolds numbers. The error is shown in Figures 4.7 and 4.2 for staggered and in-line tube banks respectively. Some of the variability in the numerical results as compared with the experiment could be due to experimental error such as the time lag to withdraw the heated element from cylindrical heater and replaced in the working section.

It is observed from the figures that the error decreases downstream of the tube bank. This shows that the local Nusselt number of numerical results get closer to experimentally obtained values in the subsequent rows downstream of the first bank of tubes.

In the case of staggered tube bank, the percentage error was estimated to be 43.32, 32.61, 22.62 and 20.52% for the first, second, third and fourth rows respectively while 36.10, 18.12, 12.89 and 34.22% correspond to first, second, third and fourth rows respectively of the in-line bank of tube arrangement.

Similarly, the staggered bank of tubes heat exchanger numerical results increased by approximately 19.11, 23.89, 16.44 and 22.08% for rows one, two, three and four respectively more than that of the in-line bank of tubes. The reason is because the tubes of staggered configuration are exposed to the main stream unlike the in-line tube exchanger where both side of tubes are in the wake region. This caused resistance to heat flow and thus lower the values of heat transfer coefficient.

Table 4.3 Comparing numerical and experimental solutions for staggered tube banks arrangement.

	Row one		**Row two**		**Row three**		**Row four**	
Throttle opening (%)	Numerical solution	Experimental solution	Numerical solution	Experimental solution	Numerical solution	Experimental solution	Numerical solution	Experimental solution
	Nu	Nu	Nu	Nu	Nu	Nu	Nu	Nu
10	20.82	25.29	20.84	28.1	20.89	30.91	20.98	31.47
20	32.97	30.91	30.04	33.72	29.31	36.53	29.31	38.77
30	54.59	30.91	51.49	35.12	50.33	38.77	50.82	41.02
40	65.42	33.72	60.89	38.21	59.12	41.02	59.82	44.67
50	74.79	36.53	69.06	38.77	66.44	43.55	67.64	45.52
60	82.81	36.53	75.59	39.34	72.63	44.96	74.02	46.36
70	89.8	36.53	81.22	40.74	77.87	46.92	79.7	47.76
80	96.43	36.53	86.7	41.58	82.73	47.76	84.86	49.45
90	102.4	36.53	91.47	41.86	87.04	48.33	89.41	50.01
100	108.7	39.34	96.37	42.15	91.53	49.17	94.36	50.01

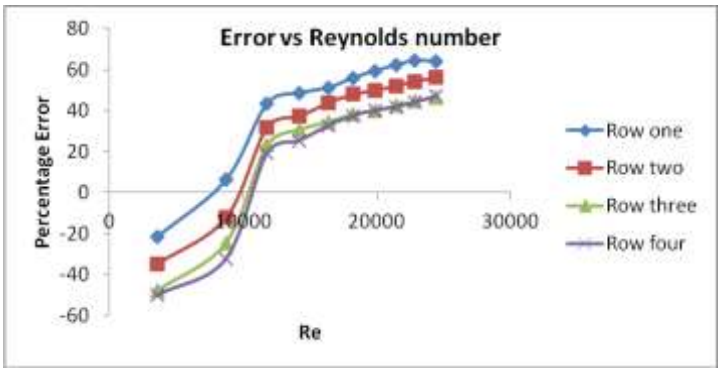

Figure 4.7 Deviation in numerical simulated Nusselt number from experimental data for staggered tube bank model.

Table 4.4 Comparing numerical and experimental solutions for in-line tube banks arrangement.

	Row one		**Row two**		**Row three**		**Row four**	
Throttle opening (%)	Numerical solution	Experimental solution	Numerical solution	Experimental solution	Numerical solution	Experimental solution	Numerical solution	Experimental solution
	Nu	Nu	Nu	Nu	Nu	Nu	Nu	Nu
10	19.389	22.48	18.90	24.73	18.893	28.1	18.634	30.91
20	30.190	26.41	28.117	30.91	28.929	35.68	28.188	37.09
30	40.674	29.78	37.196	34.56	37.196	38.77	37.340	40.46
40	49.228	32.31	43.948	36.53	46.769	39.62	41.448	41.86
50	57.102	33.44	49.813	38.21	53.569	41.02	50.339	44.11
60	64.526	34.84	54.483	39.34	59.039	42.99	55.284	44.96
70	70.017	35.4	58.598	39.9	63.877	44.39	59.725	46.64
80	77.158	36.25	62.438	40.18	68.398	45.52	63.959	47.48
90	81.908	37.09	65.838	40.46	72.393	46.08	67.794	47.76
100	89.314	37.65	69.375	41.02	76.527	46.64	71.876	48.33

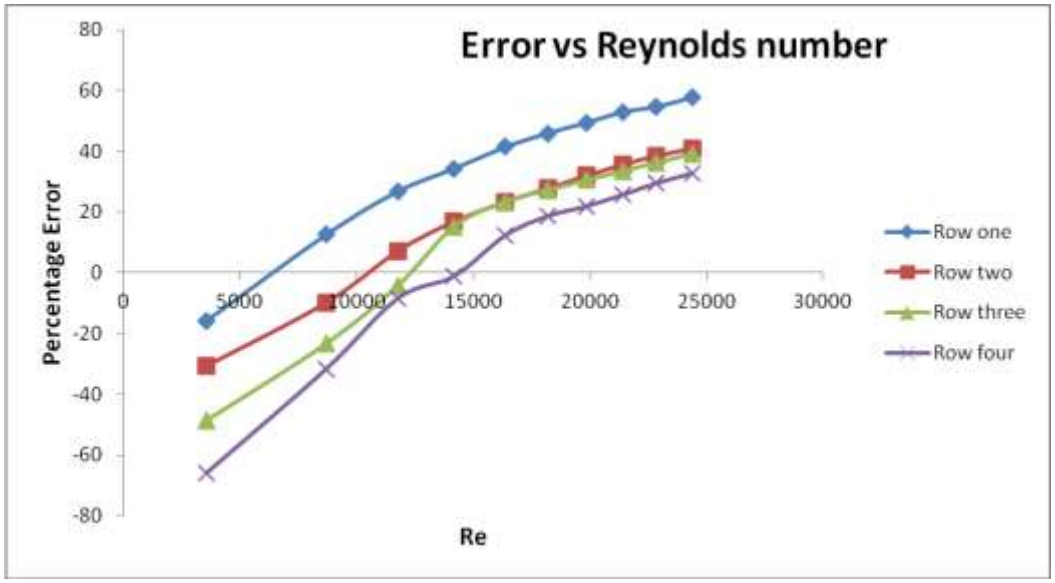

Figure 4.8 Deviation in numerical simulated Nusselt number from experimental data for in-line tube bank model.

5. CONCLUSIONS

Numerical analysis of forced convection heat transfer was performed for staggered and in-line cylindrical tube bank heat exchangers. The purpose of the work was to determine the local heat transfer and fluid flow characteristics by finite element simulation using FEMLAB 3.0 software and validate the results against experimental data.

The numerical analyses of flow and heat transfer characteristics of four rows five tubes staggered and in-line heat exchanger was performed by using FEMLAB 3.0 to create the geometry and mesh. The resulting mesh was used for running the simulation. Ten different inlet flow velocities ranging from 4.524 m/s to 31.126 m/s and corresponding to throttle opening ranging from 10% to 100% obtained from experimental work were simulated in the two different tube-type heat exchangers. Using the simulation results and some non-dimensional numbers, calculations related to heat flow was carried out to determine the Nusselt number for comparison with the experimentally obtained values used for validation.

The results of local Nusselt number predicted by simulation study show a fairly good consensus with the experimental values. For the staggered tube heat exchanger, approximately 29.77% error was found while a percentage error of approximately 25.31% was associated with in-line tube heat exchanger.

Comparative study of two different heat exchangers suggest that the velocity and Nusselt number for staggered tube heat exchanger were higher than that of in-tube heat exchanger in each row of tube banks. The staggered tube banks was approximately 20.38% higher in terms Nusselt number than the in-line tube banks.

REFERENCES

[1] Horvat Andrej, Leskovar Matjaz, Mavko Borut (2006) Comparison of heat transfer conditions in tube bundle cross-flow for different tube shapes. *International Journal of Heat and Mass Transfer* 49: 1027–1038.

[2] Zukauskas A. (1987). Heat Transfer from Tubes in Cross-flow, Advances in Heat Transfer, Vol. 8:93-160.

[3] Kays, W. S., London, A. L., (1998). Compact Heat Exchangers, 3rd Ed., Krieger Publishing Company, Malabar, Florida.

[4] Launder, B. E., Massey, T. H., (1978). The Numerical Prediction of Viscous Flow and Heat Transfer in Tube Banks, Journal of Heat Transfer, Vol. 100, pp. 565-571.

[5] Horvat, A., Mavko, B., (2005). Hierarchic Modeling of Heat Transfer processes in Heat Exchangers, *International Journal of Heat and Mass Transfer*, 48, pp. 361-371.

[6] Uguru-Okorie D. C, Ikpotokin Igbinosa, Osueke C. O and Fadare D.A (2018) Experimental Comparison of Staggered and In-Line Tube-Bank Thermal Performance. *International Journal of Mechanical Engineering and Technology (IJMET)* 9 (13):1061-1070.

[7] Marvin J. G., Huang, G. P. (1998). Status and future directions for turbulence modeling, *Sadhana*, 23:481–503.

[8] Ferziger J. H. (1987). Simulation of incompressible turbulent flows, *Journal of Computational Phys*ics, vol. 69: 1–48.

[9] Roshko A. (1993). Perspectives on bluff body aerodynamics, *International Journal of Wind Eng. Ind. Aerodyn*. 49: 79–100

[10] Kelkar K . M., Patankar S. V. (1992). Numerical prediction of vortex shedding behind a square cylinder, *International Journal of Numerical Method for Fluids, vol.* 14: 327–341

[11] Eaton B. E.(1987). Analysis of laminar vortex shedding behind a circular cylinder by computer aided flow visualization, *Journal of Fluid Mechanics,vol.* 180: 117–145

[12] Fujii M., Fujii T., Nagata T. (1984). A numerical analysis of laminar flow and heat transfer of air to inline tube banks, *Numerical Heat Trans*, vol. 7: 89–102

[13] Dhaubhadel M. N., Reddy J. N., Telionis D. P. (1986). Penalty finite element analysis of coupled fluid flow and heat transfer for in-line bundle of cylinders in cross flow, *Journal of Non-linear Mechanics*, vol. 21: 361– 373

[14] Gowda Y. and Narayana P.(1998). Finite Element Analysis of Mixed convection over In-line Tube Bundle, International Journal of Heat and Mass Transfer, Vol.41:1613–1619.

[15] Fletcher C. A. J. (1984). *Computational Galerkin methods* (New York: Springer-Verlag)

[16] Segarlind L. J. (1984). *Applied finite element analysis* (New York: Wiley)